**Master's Thesis of Engineering**

# Multicycle electrochemical lithium recovery from lithium-ion battery leachate using $LiNi_xMn_{2-x}O_4$/AC electrode

## $LiNi_xMn_{2-x}O_4$(LNMO)/AC 전극을 이용한 리튬이온전지 침출수 내 다주기 전기화학적 리튬 회수

**August 2023**


**Graduate School of Engineering**
**Seoul National University**
**Energy Systems Engineering**

**Dwira Satria Arby**

# Multicycle electrochemical lithium recovery from lithium-ion battery leachate using $LiNi_xMn_{2-x}O_4$/AC electrode

**Academic Advisor Eunhyea Chung**

**Submitting a master's thesis of**
**Engineering**

**August 2023**

**Graduate School of Engineering**
**Seoul National University**
**Energy Systems Engineering**

**Dwira Satria Arby**

**Confirming the master's thesis written by**
**Dwira Satria Arby**

**August 2023**

Chair _____(Seal)
Vice Chair _____(Seal)
Examiner _____(Seal)

# Abstract

Lithium (Li) has been known for its excellent electrochemical performance due to its increasing utilization in energy-related applications such as lithium-ion batteries (LIBs). Typically, end-of-life LIBs undergo recycling through a leaching process that yields a solution known as LIB leachate that contains lithium and other LIB materials. Among the various techniques for selectively recovering lithium from the LIB leachate, the electrochemical technique, which generally uses lithium-manganese oxide (LMO) electrodes, is one of the promising techniques. However, the stability performance of LMO is poor, primarily due to the Jahn-Teller effect of $Mn^{3+}$ in LMO. This study focuses on substituting with nickel dopant was used to reduce the manganese content of LMO. Using lithium nickel manganese oxide (LNMO) and activated carbon (AC) electrodes, lithium was selectively recovered from actual LIB leachate. The effects of operation time and current on lithium recovery from LIB leachate were studied to determine the optimal operation condition. The results demonstrate that longer operation time and higher currents increased lithium capture capacity and also increased energy consumption. Lithium recovery test using the obtained optimal operational conditions resulted in a lithium capture capacity of 1.58 mmol/g, a lithium purity of 95.22%, and an energy consumption of 2.79 Wh/mol. Additionally, the effect of nickel doping into LMO on its performance was also investigated over 20 cycles. In a 20-cycle lithium recovery test, $LiNi_{0.5}Mn_{1.5}O_4$ (LNMO-0.5) electrode showed stable lithium recovery performance, retaining approximately 97% of the initial lithium capture capacity and increasing energy consumption by approximately 7% after 20 cycles. In contrast, for pristine LMO, only about 47% of the initial lithium capture capacity was retained

after 20 cycles, and the energy consumption was approximately 65% higher than in the initial cycle. Due to the outstanding performance of LNMO, it is expected as a potential material for long-term selective lithium recovery from leachate in actual lithium-ion battery applications.

**Keyword :** Lithium recovery, electrochemical, LIB leachate, LNMO, lithium battery

**Student Number :** 2021-27252

# Table of Contents

# List of Figures

# Chapter 1. Introduction

## 1.1. Research background

Lithium (Li) is renowned for possessing excellent electrochemical performance, which has contributed to its growing utilization in energy-related applications such as lithium-ion batteries (LIB) (Talens Peiró et al., 2013). Due to the rapid development of electric vehicles, the annual lithium demand is increasing (Liu et al., 2019). Demand for lithium has nearly doubled over the past five years, particularly in the battery industry, and the growth is predicted to continue (Tabelin et al., 2021). Conventional methods of lithium recovery, such as evaporation, precipitation, adsorption, electrodialysis, and extraction with chelating materials or solvents, typically require long operating periods or involve complex multiple steps (Battistel et al., 2020). Therefore, developing more efficient lithium recovery techniques is essential to meet the skyrocketing increasing lithium demand.

The electrochemical method has proven to be an effective approach to lithium recovery because the lithium recovery rate is higher with lower energy consumption than conventional methods (Jang et al., 2021; Pasta et al., 2012). The earliest proposed lithium recovery with an electrochemical process used LMO/Pt electrolytic cells (Kanoh et al., 1993). With the rapid development of desalination technology and hybrid entropy batteries, many lithium-ion electrodes have been studied and utilized for electrochemical lithium recovery. Cathode materials, such as $FePO_4$, LMO, and $Li_{1-x}Ni_{1/3}Co_{1/3}Mn_{1/3}O_2$ (NMC), have been used for selective lithium recovery. Additionally, silver (Ag), nickel hexacyanoferrate (NiHCF), activated carbon (AC), and zinc have been utilized as counter electrodes (Kim et al., 2015;

Lawagon et al., 2019; Lee et al., 2013).

Lithium can be obtained from various sources, including hard minerals, brine lakes, and seawater (Lee & Chung, 2020). Moreover, lithium can potentially be recovered from LIB leachate. With the rapid increase in lithium battery usage, many end-of-life LIBs are discarded. Therefore, battery recycling has become one of the main interests of battery manufacturers (Jang et al., 2021). Recycling end-of-life LIBs on an industrial scale can be accomplished through hydrometallurgy, pyrometallurgy, or a combination of both methods (Tabelin et al., 2021). In the hydrometallurgical technique, strong acids are used to dissolve end-of-life LIBs during the recycling process, resulting in an acidic leachate solution called LIB leachate that contains lithium as well as other LIB materials such as manganese, nickel, and cobalt (Xu et al., 2021).

Jang et al. (2021) proposed direct lithium recovery using an electrochemical method from LIB leachate. The LMO/AC electrode system has demonstrated excellent lithium recovery performance, showing high recovered lithium selectivity for key competing ions such as manganese, nickel, cobalt, and aluminum in the LIB leachate (Jang et al., 2021). LMO has a high theoretical adsorption capacity and excellent lithium selectivity. However, its stability is poor because of the Jahn-Teller effect of $Mn^{3+}$ ($2Mn^{3+} \rightarrow Mn^{4+} + Mn^{2+}$) that can cause damage to the framework structure of LMO during the multicycle test (Haruna et al., 2022; Ouyang et al., 2009; Rodríguez et al., 2018). To overcome these drawbacks, the introduction of dopants such as Ni, Cd, Co, Cr, Al, and Mg has been explored to reduce manganese content in LMO. These dopants have been proven to form M-O bonds that are stronger than Mn-O bonds, eventually improving the stability of the material (Chen et al., 2018; Yuan et al., 2010). Among various doped materials, Ni-doped LMO or lithium nickel

manganese oxide (LNMO) is attractive because of its excellent cycle stability and high energy density (Lee et al., 2017). Studies focusing on lithium recovery from brine using LNMO have demonstrated its effectiveness in separating lithium ions from other competing ions ($Na^+$, $K^+$, $Mg^{2+}$, and $Ca^{2+}$) and confirmed the high stability of the cathode material (Lawagon et al., 2019; Shang et al., 2021).

## 1.2. Research objective

In this study, LNMO was utilized as the working electrode material for the electrochemical lithium recovery from LIB leachate. LNMO showed high lithium selectivity and stability over multiple cycles during tests conducted with a brine sample (Shang et al., 2021). On the other hand, AC was chosen as the counter electrode material due to its cost-efficiency compared to other alternatives (Porada et al., 2013). The selectivity and purity of recovered lithium, compared to other competing ions (Ni, Mn, and Co) in the LIB leachate, were also examined. Additionally, the effect of nickel doping level in LNMO on lithium recovery performance and stability was investigated. The results demonstrated that selective electrochemical recovery of lithium from LIB leachate using LNMO exhibited greater stability in a multicycle operation when compared to pristine LMO.

# Chapter 2. Literature Review

## 2.1. Electrochemical lithium Recovery

In the early 1990s, Kanoh et al. performed the initial electrochemical trapping of Li cations from a source solution into a battery material using the intercalation of Li, which is the most common working mechanism of rechargeable Li-ion batteries. They employed spinel λ-$MnO_2$ as a working electrode and a Pt wire as a counter electrode. The intercalation and de-intercalation process is summarized as

$$2\lambda - MnO_2 + 0.5Li^+ + 0.5e^- \leftrightarrow Li_{0.5}Mn_2O_4 \quad (1)$$

$$Li_{0.5}Mn_2O_4 + 0.5Li^+ + 0.5e- \leftrightarrow LiMn_2O_4 \quad (2)$$

Generally, electrochemical lithium recovery involves four steps. Firstly, Li cations from a feed electrolyte, brine or LIB leachate, are selectively intercalated into a Li-capturing electrode by applying a current. Secondly, the solution is replaced with a recovery solution, where Li is released. Thirdly, by switching the current direction, the Li cations are released into the recovery solution. Lastly, the Li source solution is once again flushed in the cell, and the cycle can recommence from the beginning. By repeating these cycles, the concentration and purity of Li in the recovery solution are increased.

The key advantage of the electrochemical method is that this method employs the application of current as the driving force for lithium capture, obviating the need for any other chemical species to regenerate the active material. Although the capacity of battery materials is not significantly different from that of the adsorption materials employed in the past, the time required for capturing the same amount of Li is much lower compared to the adsorption process. This is a direct outcome of the

current application to the electrode, which amplifies the Li capturing rate. However, the porosity and hygroscopic properties of the materials limit the final Li concentration, as the solution adsorbed into the electrodes will mix with the enriched Li solution at each cycle. Nonetheless, this issue can be addressed by flushing and utilizing a cell design with small dead volumes and a compact electrode stack (Lee et al, 2013).

## 2.2. Electrode materials

### 2.2.1. Lithium nickel manganese oxide (LNMO)

The materials that have been used as lithium recovery electrodes thus far are the same as those employed as cathode electrodes in Li-ion batteries, which guarantees their ability to adsorb or insert lithium. The LMO electrode has proven excellent lithium recovery performance, showing high recovered lithium selectivity for key competing ions such as manganese, nickel, cobalt, and aluminum in the LIB leachate (Jang et al., 2021). Considerable effort has been dedicated to addressing the drawbacks of LMO, namely, Mn dissolution in the electrolyte and poor electronic conductivity. To overcome these issues, several methodologies such as morphology and particle size control, surface modification, and doping have been studied extensively.

$LiNi_{0.5}Mn_{1.5}O_4$ (LNMO) can be produced by doping the sites of manganese spinel with nickel, as Mn in LMO is the main cause of the unstable electrochemical performance. Research into lithium recovery from brine using LNMO has demonstrated its effectiveness in separating lithium ions from other competing ions such as $Na^+$, $K^+$, $Mg^{2+}$, and $Ca^{2+}$. This has also verified the exceptional stability of the cathode material (Lawagon et al., 2019; Shang et al., 2021).

### 2.2.2. Counter electrodes

Various materials such as platinum, silver, activated carbon, and Prussian blue analogue electrodes are used as counter electrodes for electrochemical lithium recovery from brine.

Kanoh et al. (1993) were the pioneers in this field and used a Pt wire or sheet as the counter electrode, which has also been used in recent publications. Pt is inert

to Li and other ions present in the brine, and thus, water oxidation and reduction occur during the extraction and recovery steps, respectively. However, the high cost of this noble metal and the increment in energy required for the process due to the electrochemical potential of these reactions limits its commercial use. Additionally, the local pH evolution near the electrode's surface can lead to the precipitation of dissolved ions.

Silver electrodes are another common alternative of Pt for counter electrodes in lithium recovery from brine due to their ability to capture chloride ions, which are the main anions in brine. However, the relatively high cost of silver and its solubility under certain conditions make it less desirable as a counter electrode material.

The activated carbon electrode is commonly utilized in electrochemical water desalination (Liu et al., 2019) because of its affordability, high surface area, and excellent electrical conductivity. It is also used as a counter electrode for electrochemical lithium recovery from brine (Lee et al., 2017).

# Chapter 3. Methodology

## 3.1. Materials and reagents

Lithium acetate (≥ 99% purity $LiAc.2H_2O$), nickel (II) acetate (≥99% purity $Ni(Ac)_2.6H_2O$), and manganese (II) acetate (99.99% purity $Mn(Ac)_2.4H_2O$) from Sigma Aldrich were used as precursors in the preparation of LNMO. Citric acid (≥99.5% purity $C_6H_8O_7.H_2O$) was used as a chelating agent during LNMO fabrication. N-methyl pyrrolidone (≥99.5% purity NMP) and Polyvinylidene fluoride (PVDF) were used as solvent and binder, respectively, during electrode fabrication. Super P carbon black from Timcal, Switzerland, was also added during electrode fabrication to improve the material conductivity. Activated carbon (CEP-21K; Power Carbon Technology Co., Korea) was used as the counter electrode.

## 3.2. LNMO fabrication and characterization

LNMO was synthesized through solid-state reaction according to a protocol adopted from the literature (Tian & Yuan, 2009). Lithium acetate, nickel (II) acetate, manganese (II) acetate, and citric acid were ground in a mortar at room temperature for 1 hour to a molar ratio of 1: $x$ : 2-$x$ :3. The amount of nickel doping in LNMO was varied between 0 and 0.75 molar ratio. During the grinding process, a solid-state reaction occurred along with the gradual release of water from the crystals, giving the mixture a wet, paste-like texture. The paste-like mixture was dried in a vacuum oven at 80°C for 6 hours and then calcined at 650°C for 12 hours. The LNMO powder without nickel acetate ($x$ = 0) was named LMO and used as a control. The LNMO powder samples with molar ratios of 0.25, 0.5, and 0.75 nickel acetate were named LNMO-0.25, LNMO-0.5, and LNMO-0.75, respectively.

The crystal structure of the powder samples (LMO, LNMO-0.25, LNMO-0.5, and LNMO-0.75) was determined using X-ray diffraction (Rigaku D/Tex Ultra250 X-ray powder diffractometer) over the $2\theta$ range of 10º–80º. The microstructure of the powder was further evaluated using field-emission scanning electron microscopy (FE-SEM, JSM-7800F Prime, JEOL Ltd, Japan). In addition, manganese valence distribution was determined using X-ray photoelectron spectroscopy (ESCA II Axis Supra, Kratos, UK).

## 3.3. Electrode fabrication and characterization

LNMO electrodes were made by mixing LNMO powder, PVDF, and carbon black (80:10:10 wt.%) in an NMP solvent to form a slurry. Then, using a doctor blade, the slurry was coated on a titanium plate with an effective area of 16 $cm^2$ (4 cm × 4 cm). The titanium plate coated by the LNMO slurry was dried in an oven at 120°C under vacuum conditions for 12 hours. As the counter electrode, the AC electrode was made by mixing AC powder and PVDF (90:10 wt%) in an NMP solvent to form a slurry. The slurry was poured on a titanium plate and thinly coated using a doctor blade. The titanium plate coated by the AC slurry was dried at 120°C for 2 hours under room pressure and at 80°C for 2 hours under vacuum conditions.

Electrochemical characteristics were determined at room conditions using an electrochemical analyzer (Zive SP1, WonA Tech). Using a three-electrode setup, cyclic voltammetry experiments were performed in 1 M $Li_2SO_4$ solution at a scanning rate of 0.5 mV/s over a potential range of 0 to 1.2 V. The three-electrode setup contained an LNMO working electrode, an AC counter electrode, and an Ag/AgCl reference electrode.

## 3.4. Lithium recovery experiment

The LNMO electrodes were set in a 30 mM LiCl solution and delithiated (before the lithium recovery experiment) with the three electrodes (mentioned above) at a constant current of 0.1 A/g until the electric voltage reached 1.1 V.

The lithium recovery experiment used a two-electrode system (LNMO working electrode and AC counter electrode) with 20 mL of LIB leachate flowing in a batch system (Figure 3.1). The LIB leachate was a synthetic solution based on the concentration (Table 3.1) provided by the industry. A nylon spacer was placed between the working and counter electrodes to provide a channel for the solution. In addition, an anion exchange membrane (Neosepta, Astom Co., Japan) was placed in front of the counter electrode to prevent cations from being adsorbed to the counter electrode. The space between the two electrodes was approximately 2 mm. Silicone gasket is placed between the layers of the electrochemical cell assembly to ensure that there is no leakage from the experimental setup. By placing silicone gaskets between the layers, a tight and secure seal is created, preventing any liquid from leaking out and maintaining the integrity of the experiment.

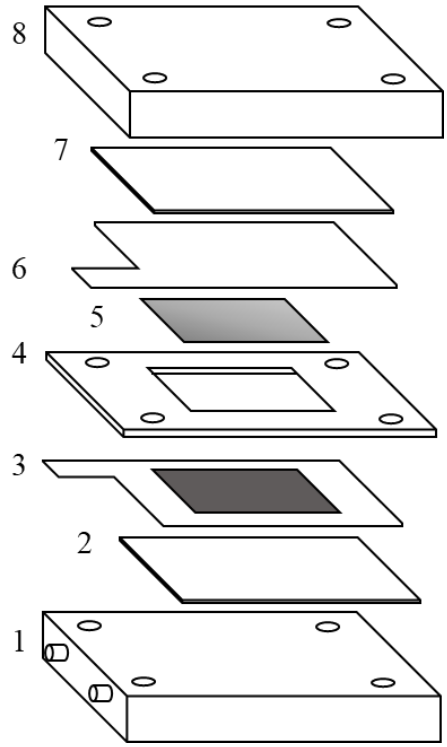


**Figure 3.1.** Diagram of the electrochemical cell (1 and 8: 6 cm x 6 cm plexiglass shells; 2, 4, and 7: 6 cm x 6 cm silicone gaskets and spacer; 3: LNMO electrode on 6 cm x 6 cm Ti plate; 5: 4 cm x 4 cm anion exchange membrane; 6: AC electrode on 6 cm x 6 cm Ti plate).

**Table 3.1.** Concentration of ions in the LiB leachate

| | mg/L | mM |
|---|---|---|
| Li | 13128 | 1891 |
| Ni | 59877 | 1020 |
| Co | 31471 | 534 |
| Mn | 17936 | 326 |
| Na | 14998 | 652 |
| Ca | 158 | 3.94 |
| Fe | 267 | 4.78 |
| Mg | 124 | 5.10 |
| Al | 3087 | 114 |
| Cu | 1015 | 16.0 |

The lithium recovery process consists of several cycles. Each cycle includes two consecutive steps, i.e., lithium capture step and lithium release step (Figure 3.2). During the capture step, the LIB leachate was pumped into the assembly, and cations were captured into the LNMO electrode at a constant negative current for a specific duration. Before the next step, the inner part of the assembly was washed by circulating deionized water. In the release step, 30 mM KCl solution was pumped into the electrode assembly as the receiving solution. Cations were releaseded from the electrodes at a constant positive current for certainty. The concentrations of the ions in the recovery solution were examined by ICP analysis (ICP-OES Avio 220 Max).

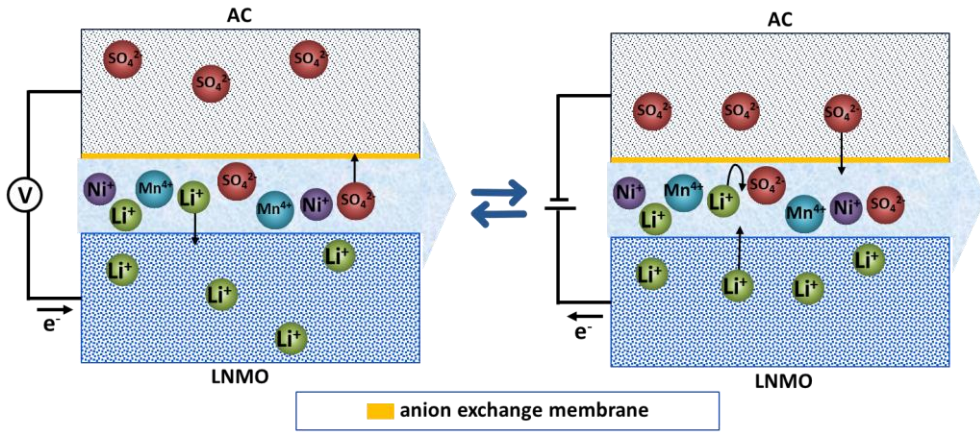


**Figure 3.2.** Conceptual diagram of lithium capture (left) and release (right) processes using LNMO/AC electrodes.

The ion capture capacity (mmol/g) was calculated using Eq. (3)

$$Ion\ capture\ capacity = \frac{C_M \cdot V}{m} \quad (3)$$

where $C_M$ (mM) is the concentration of ions after being released, m (g) is the mass of the LNMO loaded on the titanium plate, and V (L) is the recovery solution volume.

The lithium selectivity coefficient over other major competing cations was then calculated as follows:

$$Lithium\ selectivity\ coefficient = \frac{C_{Li}}{C_M} \quad (4)$$

where $C_{Li}$ and $C_M$ are the concentrations of lithium and other cations, respectively, in the recovery solution.

The lithium purity (%) was determined by dividing the concentration of lithium ($C_{Li}$) by other cations, including lithium ($\Sigma C_M$), in the recovery solution.

$$Lithium\ purity = \frac{C_{Li}}{\sum C_M} \times 100\% \quad (5)$$

The molar energy consumption (W, Wh/mol) was calculated using Eq. (6).

$$Energy\ consumption = \frac{\int \Delta E dq}{V \cdot C_{Li}} \quad (6)$$

where ΔE (V) is the charge-dependent potential profile (q, C).

The amount of dissolved manganese (mmol/g) was calculated using Eq. (8).

$$Dissolved\ manganese\ amount = \frac{C_{Mn} \cdot V}{m} \quad (7)$$

where $C_{Mn}$ (mM) is the concentration of manganese ions in the cycled solution, m (g) is the mass of the LNMO loaded on the titanium plate, and V (L) is the cycled volume.

# Chapter 4. Result and Discussion

## 4.1. Material characterization

A series of sharp peaks can be observed in the XRD patterns of LNMO and LMO samples, indicating that the samples are highly crystalline (Figure 4.1). The peaks of LNMO and LMO match with the spinel minerals found in the ICDD database (PDF-010-080-2984 for LNMO and PDF-01-074-9872 for LMO) that are attributed to a face-centered cubic crystal structure. As the amount of nickel in LNMO increases, the peaks shift to a slightly higher angle ($2\theta$) than the LMO peaks. The addition of $Ni^{2+}$ ($r$ = 0.69 Å) to the crystal structure increases $Mn^{4+}$ ($r$ = 0.53 Å) with a smaller radius and decreases $Mn^{3+}$ ($r$ = 0.64 Å) with a larger radius to maintain the electroneutrality of the system, resulting in a smaller cell volume. The findings from the XRD patterns are also attributed to Ni-O bonds that are stronger than the main Mn-O chemical bonds and to Ni-O bonds that are smaller than Mn-O bonds (dos Santos Junior et al., 2020; Yu et al., 2019).

The presence of some peaks in the XRD patterns of LNMO 0.75 suggests the potential existence of impurities. These impurities could be attributed to the calcination temperature during the fabrication of the material. It is known that higher calcination temperatures, typically above 800°C, can help prevent the formation of impurities in LNMO. By using higher calcination temperatures during the material fabrication process, it is possible to enhance the crystal structure purity of LNMO. The higher temperature promotes more complete solid-state reactions, allowing for better formation of the desired spinel structure and reducing the presence of impurities in the final product.

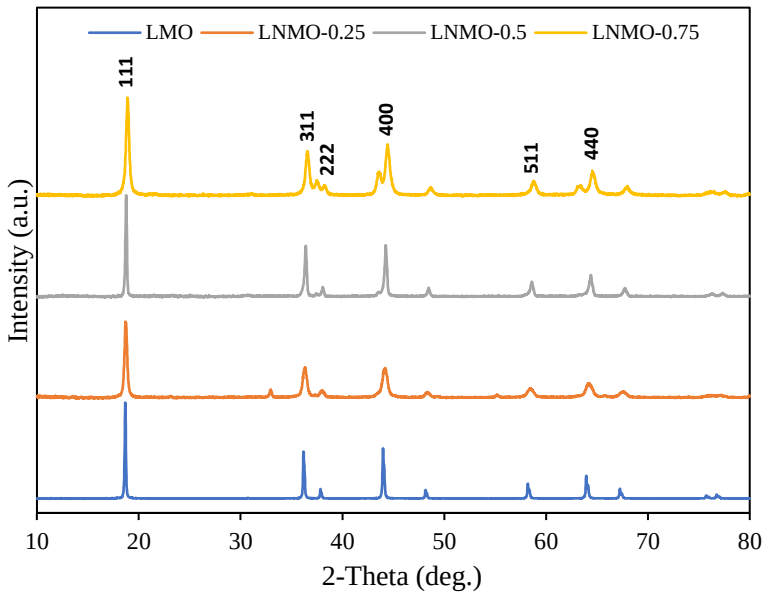


**Figure 4.1.** XRD patterns of LMO, LNMO-0.25, LNMO-0.5, and LNMO-0.75.

FE-SEM was used to characterize the morphology of LNMO and LMO. All samples contained irregularly shaped nanoparticles, with particle sizes ranging from 60 to 100 nm for LNMO and LMO (Figure 4.2). However, some nanoparticles were larger than 500 nm for LMO. LMO exhibited agglomeration of tiny particles into large nanoparticles (Figure 4.2a), resulting in diverse particle sizes. As the nickel content increased, the agglomeration gradually decreased, and the particle size decreased proportionally (Figure 4.2b-d). Nickel doping into the LMO matrix increased crystal nuclei, decreased the agglomeration phenomenon, and increased crystallization in all doped samples (Chemelewski et al., 2013; Yu, 2018), consistent with a shift to higher XRD angles.

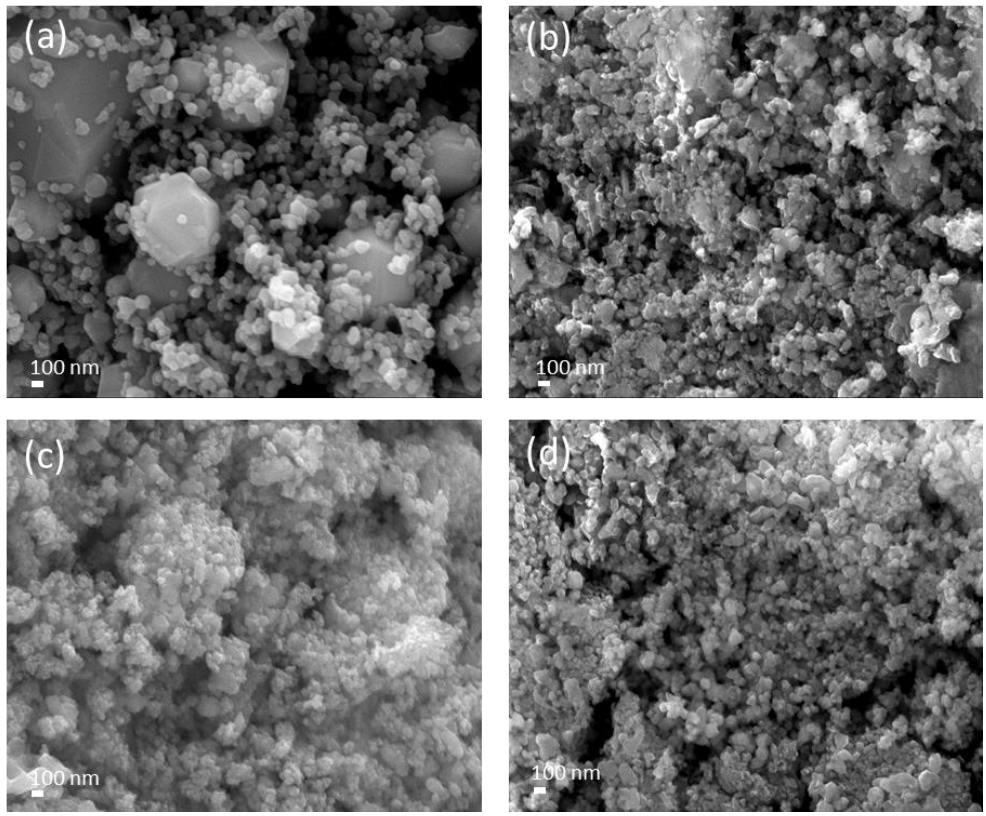


**Figure 4.2.** FE-SEM images of (a) LMO, (b) LNMO-0.25, (c) LNMO-0.5, and (d) LNMO-0.75 samples.

XPS analysis was performed to observe the valence distribution of manganese in the LMO, LNMO-0.25, LNMO-0.5, and LNMO-0.75 samples. There are 2 manganese peaks based on the XPS spectra of the samples, which are $Mn2p_{3/2}$ and $Mn2p_{3/2}$ peaks (Figure 4.3a-d). $Mn2p_{3/2}$ peak is often used to determine the oxidation state of Mn in a material, while the $Mn2p_{1/2}$ peak can provide information on the spin-orbit coupling and crystal field effects in the Mn atom. Therefore, the XPS spectra of $Mn2p_{3/2}$ were deconvoluted to determine the relative amount of $Mn^{4+}$ and $Mn^{3+}$ in all samples (Figure 4.4a-d). The results showed that nickel doping reduced the amount of $Mn^{3+}$ ions while the amount of $Mn^{4+}$ ions increased. As the amount of nickel doping increased, the amount of $Mn^{3+}$ ions decreased, and the amount of $Mn^{4+}$ ions increased. These results implied that nickel doping could inhibit the formation of $Mn^{3+}$ in the lattice and is accompanied by the development of $Mn^{4+}$ ions. As a result, $Mn^{3+}$ accelerated the dissolution of manganese during electrochemical cycling, eventually affecting the electrochemical performance and stability of the cathode materials (Tang et al., 2014). In addition, based on Capsoni et al. (2001), the Jahn-Teller effect can be suppressed when the ratio $r \geq 1.18$ ($r = [Mn^{4+}]/[Mn^{3+}]$). Using the deconvoluted XPS spectrum data, the *r*-value of LMO, LNMO-0.25, LNMO-0.5, and LNMO-0.75 were 1.17, 1.79, 2.77, and 3.19, respectively. Therefore, the Jahn-Teller effect may occur on LMO electrodes during electrochemical cycling based on *r*-values, affecting its performance, and stability. concluded

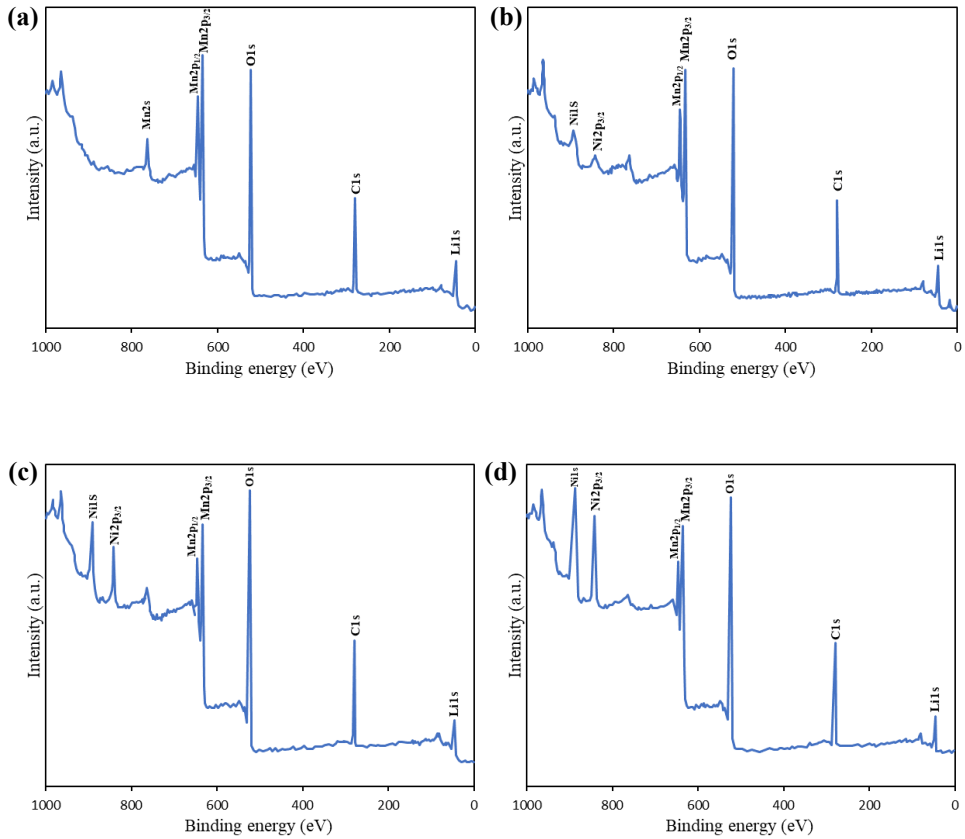


**Figure 4.3.** XPS spectra of (a) LMO, (b) LNMO-0.25, (c) LNMO-0.5, and (d) LNMO-0.75

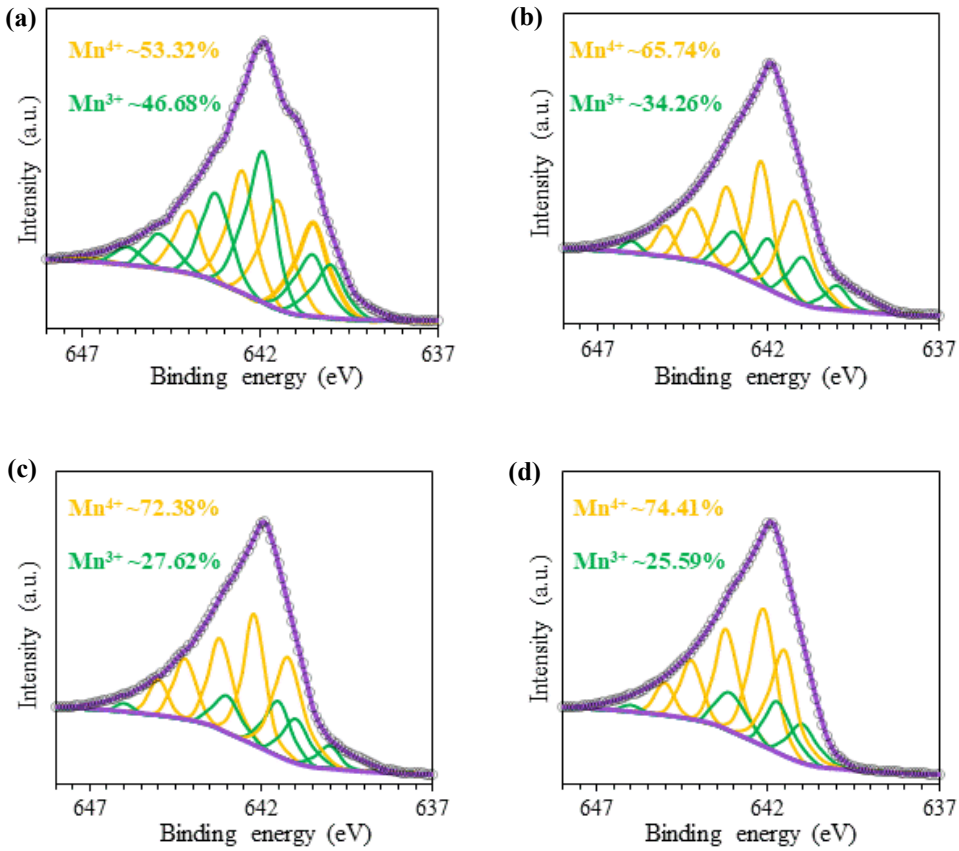


**Figure 4.4.** $Mn2p_{3/2}$ XPS spectra of (a) LMO, (b) LNMO-0.25, (c) LNMO-0.5, and (d) LNMO-0.75.

## 4.2. Material electrochemical properties

The electrochemical characteristic of LNMO and LMO was tested by CV in 1 M $Li_2SO_4$ solution. The CV of LNMO and LMO electrodes at a scan rate of 0.5 mV/s showed a couple of peaks in each reduction and oxidation step (Figure 4.5). The oxidation peaks in the positive scan between 0.7 and 1.0 V can be attributed to the de-intercalation of lithium from LNMO electrodes. During this oxidation process (positive scan) lithium ions are released from the electrode and enter the electrolyte solution. On the other hand, two reduction peaks in the negative scan appeared between 0.9 V and 0.5 V, ascribed to lithium intercalation from the solution. During this reduction process (negative scan) the LNMO electrode acts similar as an adsorbent, attracting and capturing lithium ions from the electrolyte solution. The observed pairs of redox reactions for LNMO-0.5 can be attributed to the following reactions:

$$\lambda - Ni_{0.5}Mn_{1.5}O_4 + 0.5Li^+ + 0.5Li^- \leftrightarrow Li_{0.5}Ni_{0.5}Mn_{1.5}O_4 \quad (8)$$

$$Li_{0.5}Ni_{0.5}Mn_{1.5}O_4 + 0.5Li^+ + 0.5Li^- \leftrightarrow LiNi_{0.5}Mn_{1.5}O_4 \quad (9)$$

The similar electrochemical behavior between LNMO and LMO is possibly due to the similarity in the crystalline structure (Santhanam & Rambabu, 2010). The CV results validate the suitability of LNMO and LMO electrodes for subsequent electrochemical lithium recovery tests, confirming their ability to facilitate the capture and release of lithium ions during the electrochemical process.

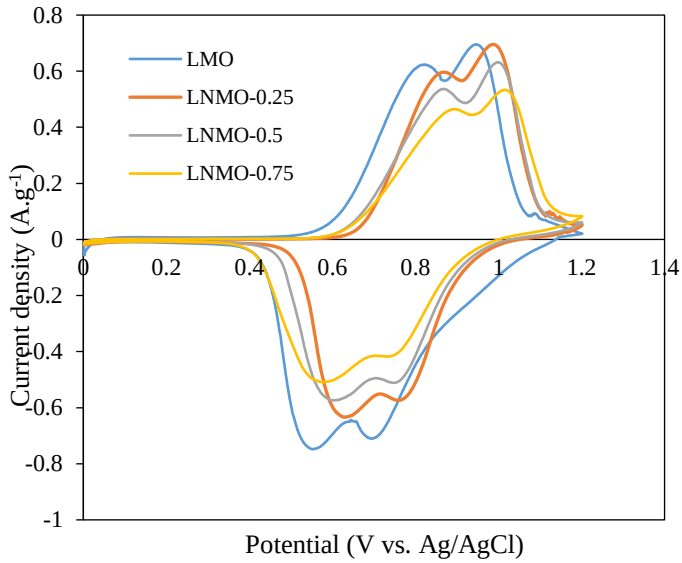


**Figure 4.5.** The CV of LMO, LNMO-0.25, LNMO-0.5, and LNMO-0.75 in 1 M $Li_2SO_4$.

## 4.3. Electrochemical lithium recovery from LIB leachate

### 4.3.1. Effects of operating current changes on lithium recovery

Lithium recovery was performed using LNMO-0.5/AC electrode at I = ±0.075–0.175 A/g in LIB leachate solution for 20 min/step. Increasing the operating current increased the lithium capture capacity (Figure 4.6a). The lithium capture capacities were 1.34, 1.43, 1.58, 1.75, and 1.97 mmol/g at the current densities of 0.075, 0.100, 0.125, 0.150, and 0.175 A/g, respectively. It is evident that an increase in current density increases the driving force for lithium recovery and, eventually, lithium capture capacity. The highest lithium purity of 95.55% from the recovery process was achieved at 0.15 A/g. The lithium purity trend increased until the current was 0.15 A/g but started to decline after that (Figure 4.6c). This trend indicated that above a certain current density, the capture and release of cations, unfavorable to lithium purity, were promoted in the electrochemical lithium recovery process.

The selectivity of lithium over major competing cations (Mn, Co, Ni, and Na) was found to increase with increasing current up to 0.15 A/g and decrease afterward. The selectivity of lithium over low-concentration ions appeared not to be affected by changes in operating current (Figure 4.6b). The selectivity of lithium over cobalt ions was significantly higher than other major coexisting ions, possibly due to the lower concentration of cobalt in the LIB leachate than other major coexisting cations.

Energy consumption per cycle of the lithium recovery process increased with increasing current density (Figure 4.6d). These results indicate that higher current density results in higher lithium capture capacity but higher energy consumption.

Considering these results, lithium recovery is preferable at high operating currents. However, high operating currents can cause side reactions and electrode

degradation in multicycle lithium recovery. Furthermore, the operating current was limited to the operating window of the LIB leachate, where hydrolysis did not occur. Therefore, the current was fixed at 0.125 A/g in subsequent experiments.

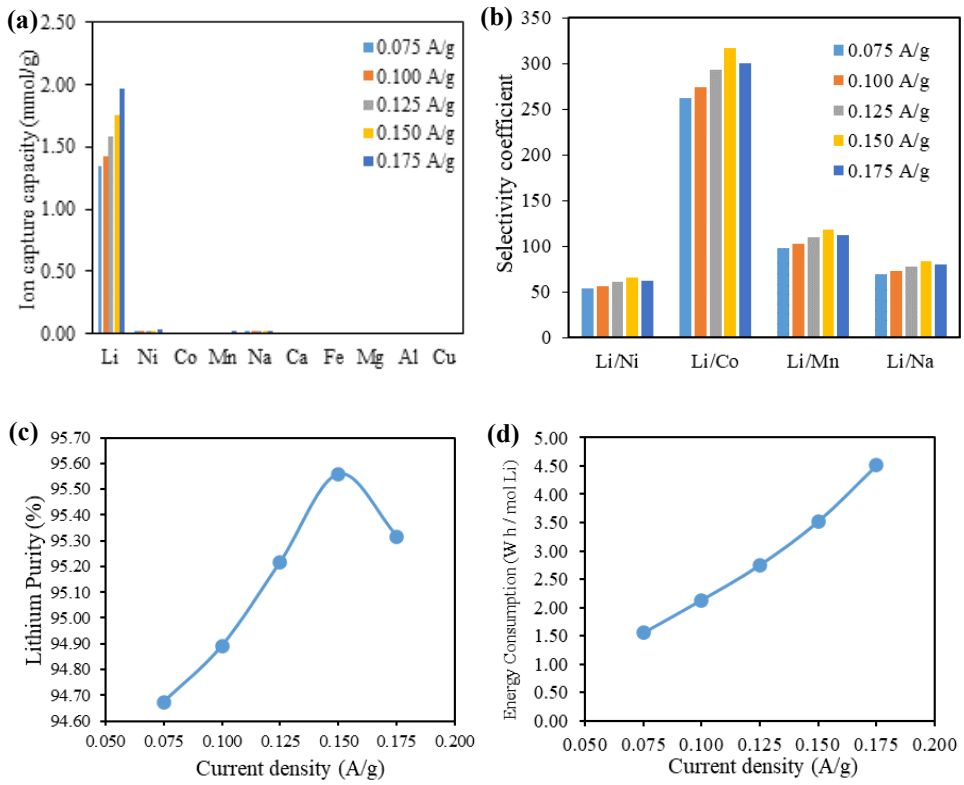


**Figure 4.6.** Lithium recovery by LNMO-0.5/AC at varied current densities (operated a 20 min/step): (a) capture capacity of all cations, (b) selectivity coefficient of lithium over major cations, (c) lithium purity trend, and (d) energy consumption trend.

### 4.3.2. Lithium recovery at varied operation time

Lithium was recovered using LNMO-0.5/AC at a current density of 0.125 A/g and an operating time of 5–25 minutes for each capture and release process of LIB leachate.

The lithium capture capacity increased significantly with increasing operation time (Figure 4.7a), reaching 0.61, 1.02, 1.35, 1.58, and 1.65 mmol/g at 5, 10, 15, 20, and 25 min/step, respectively. The capture capacities of other coexisting ions also increased with time. This indicates that the overall capture capacity of the electrode increased over time during the capture step. Although the capture capacity increased dramatically over time, the capture rate decreased gradually. This decrease can be attributed to the maximum ion capture capacity of the cathode, which is affected by the operating current. When the recovery process reached the maximum capture capacity, the capture rate slowed down. The maximum ion capture capacity may vary with the operating current because the capture capacity increases steadily as the operating current increases.

Lithium purity and selectivity increased slightly with increasing operating time (Figure 4.7b, c). The slight increase means that the rate of lithium recovered over time is faster than the recovery rate of competing ions in the LIB leachate. The molar energy increased from 1.42 to 3.41 W h/mol Li with increasing operating time (Figure 4.7d).

Lithium recovery performance improves with a longer operating time; however, the electrochemical stability window of the LIB leachate limits the range of acceptable operating times. Furthermore, as lithium capture proceeds, the number of intercalation sites on the LNMO electrode gradually decreases. As a result, the activation overvoltage increases, and the electrode potential may exceed the limit of

electrochemical stability. Moreover, the recovery rate decreases, and energy consumption increases over time. Therefore, in this study, the optimal operating time was limited to 20 min/step in subsequent experiments.

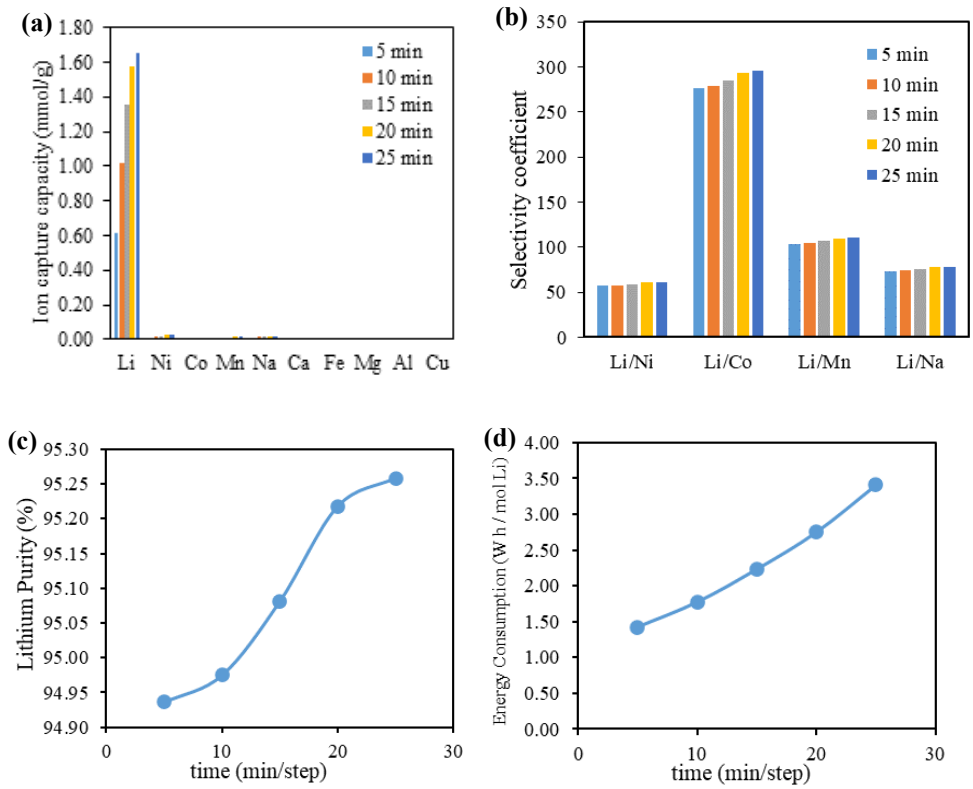


**Figure 4.7.** Lithium recovery with LNMO/AC at varying operating times (i = 20 A/g): (a) capture capacity of all cations, (b) selectivity coefficient of lithium over major cations, (c) lithium purity trend, and (d) energy consumption trend.

## 4.4. Nickel doping effect on lithium recovery performance

Twenty-cycle experiments of lithium capture and release ($i$ = 0.125 A/g, 20 min/step, AC counter electrode) demonstrated the steady effect of nickel doping in LMO electrodes on lithium recovery performance, particularly its stability for lithium recovery from the LIB leachate in multicycle tests. Each cycle consisted of a capture step and a release step. Fresh LIB leachate and receiving solution were used in each cycle.

In the initial cycle, the LMO electrode showed higher lithium capture capacity than nickel-doped LMO. However, the lithium capture capacity of the LMO electrode decreased rapidly with each cycle, retaining only 46% of its lithium capture capacity after 20 cycles. One of the nickel-doped LMOs (LNMO-0.25) also showed a decrease and retained almost 71% of its lithium capture capacity after 20 cycles. Meanwhile, the other nickel-doped LMO (LNMO-0.5 and LNMO-0.75) maintained stable lithium capture capacity through the $20^{th}$ cycle. LNMO-0.5 and LNMO-0.75 retained about 97% of their lithium capture capacity after 20 cycles (Figure 4.8).

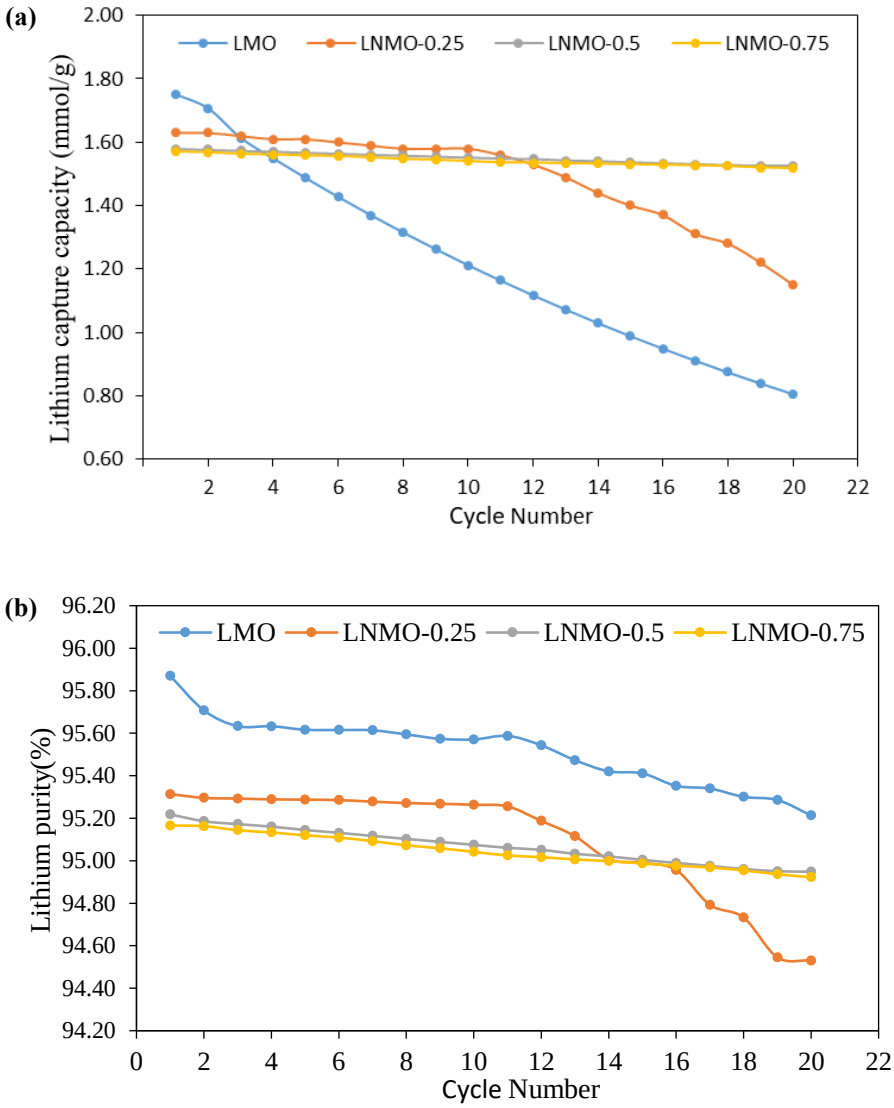


**Figure 4.8.** Multicycle performance of LMO, LNMO-0.25, LNMO-0.5, and LNMO-0.75 for lithium recovery (i = 0.125 A/g and t = 20 min step-1) from the LIB leachate: (a) lithium capture capacity profile and (b) lithium purity profile.

For LNMO-0.5 and LNMO-0.75, a slight increase in calculated molar energy consumption from 2.75 to 2.93 Wh/mol Li and from 2.79 to 2.96 Wh/mol Li, respectively, was observed with increasing cycles (Figure 4.9). In contrast, the pristine LMO electrode showed a significant increase in molar energy consumption by approximately 65% at the $20^{th}$ cycle compared to the initial cycle. In a cumulative total of 20 cycles, 0.95, 1.16, 1.21, and 1.20 mmol of lithium was adsorbed from the LIB leachate with the total energy consumption of 0.00282, 0.00329, 0.00343, and 0.00345 Wh for LMO, LNMO-0.25, LNMO-0.5, and LNMO-0.75 electrodes, respectively.

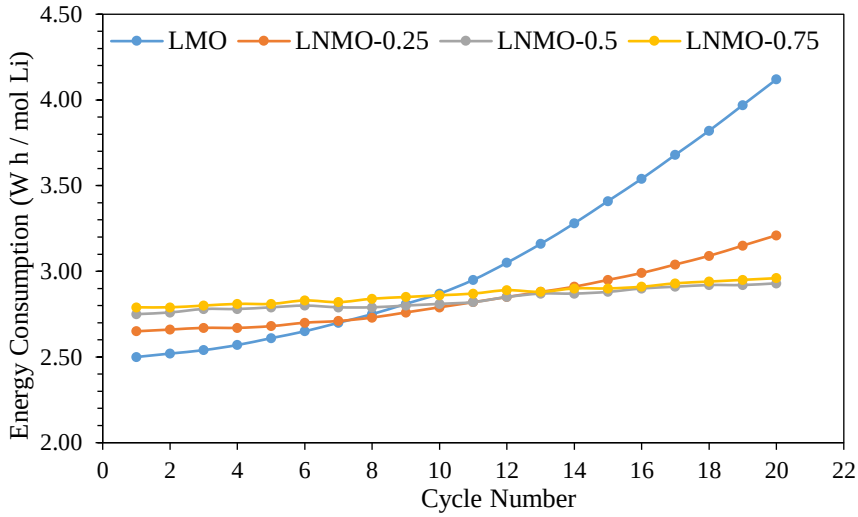


**Figure 4.9.** Multicycle performance of LMO, LNMO-0.25, LNMO-0.5, and LNMO-0.75 for lithium recovery (i = 0.125 A/g and t = 20 min step-1) from the LIB: energy consumption profile over 20 cycles.

A twenty-cycle lithium recovery test was also conducted from a solution containing only lithium ions to observe manganese dissolution from the electrode. In this test, the same solution was cycled until the final cycle. As a result, manganese was not detected during the ICP spectroscopy of the recovery solution from the multicycle test for LNMO-0.5 and LNMO-0.75

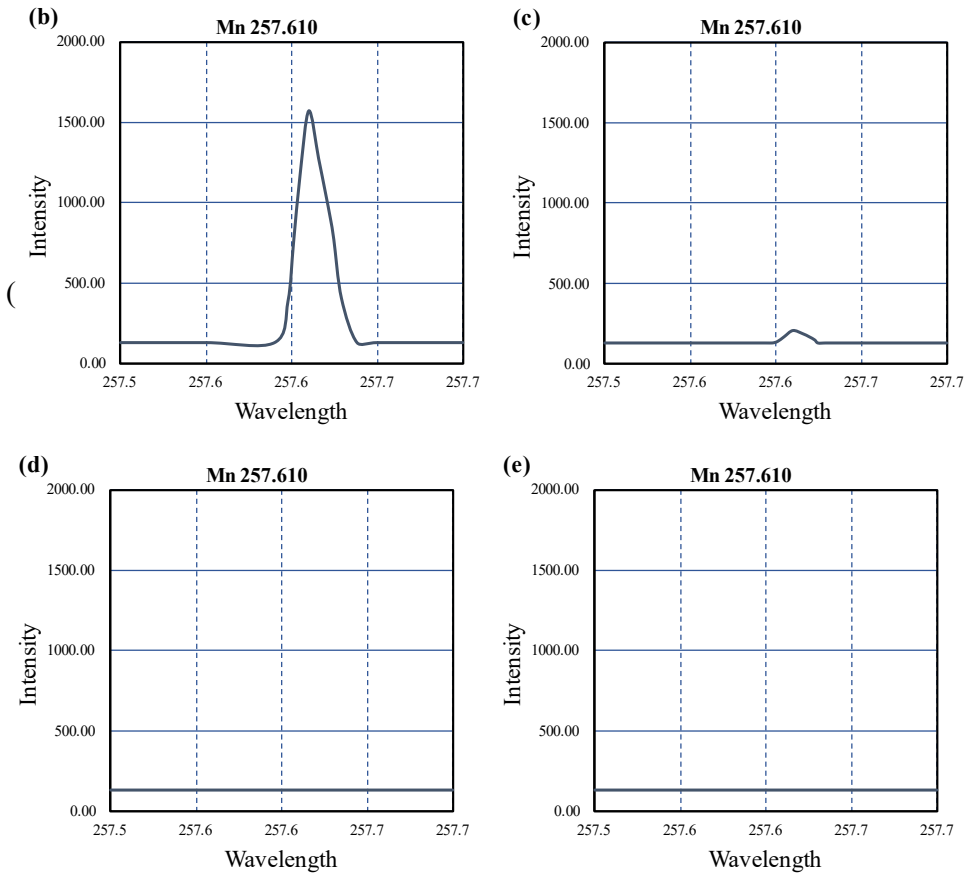


Figure 4.10d-e). Manganese peak slightly appear based on the ICP spectra data for the recovery solution from the multicycle test of LNMO-0.25, but the manganese concentration was still unquantifiable by the ICP (Figure4.10c). This result implied that there is a high possibility that a very low concentration of manganese from the electrode is dissolved into the solution. Thus, affecting the stability of LNMO-0.25 during the multicycle test, as mentioned in the previous paragraph. Meanwhile,

manganese peak was observed in the multicycle test for the pristine LMO electrode (Figure 4.10b). Furthermore, it was observed that the amount of manganese dissolved increased as the cycles proceeded (Figure 4.10a).

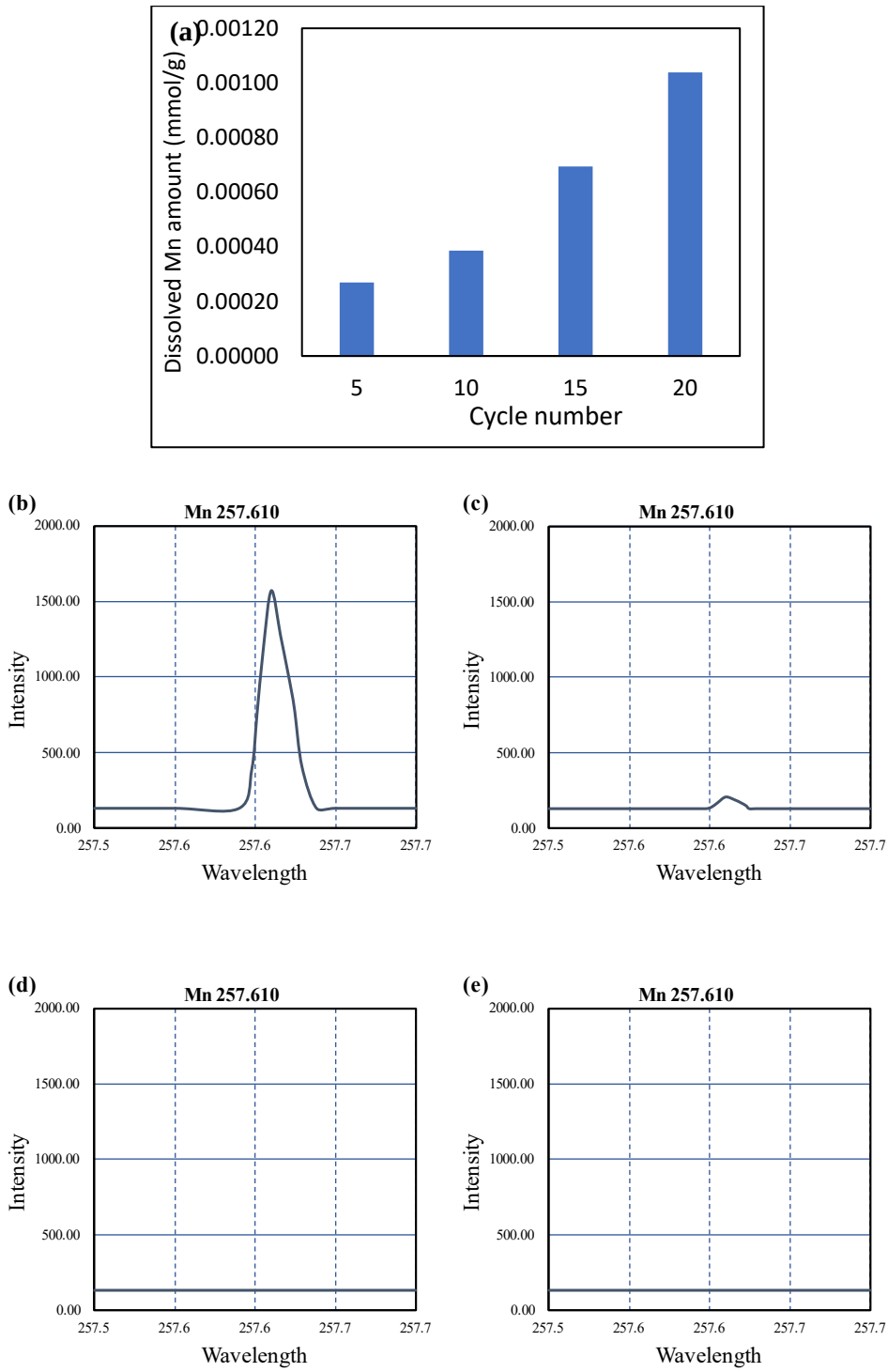


**Figure 4.10.** (a) Amount of dissolved manganese in LMO during multicycle lithium recovery test and the manganese spectra from ICP of the 20$^{th}$ cycle recovery solution (b) LMO, (c) LNMO-0.25, (d) LNMO-0.5, (e) LNMO-0.75.

These results suggest that higher nickel doping levels improve the stability of long-term electrochemical lithium recovery. When nickel is doped into LMO, $Mn^{3+}$ is replaced by $Ni^{2+}$ in the crystal structure. The substitution increases $Ni^{2+}$ and decreases $Mn^{3+}$. Since $Mn^{3+}$ is soluble, it is susceptible to the Jahn-Teller effect in the electrochemical process, causing further damage to the crystal structure (Guan et al., 2011; Haruna et al., 2022; Thackeray, 1999).

For efficient large-scale recovery of lithium using electrochemical cell in an industrial application, some cell assembly design which possibly suitable are: (1) Stacked or parallel electrode assemblies, where multiple electrode pairs are placed in series, allowing for efficient and larger capacity ion removal across the entire stack; (2) The Flow Electrode design where the electrode material is directly integrated into the flow channels.

# Chapter 5. Conclusions

The potential of nickel-doped LMO (LNMO) for multicycle electrochemical selective recovery of lithium from lithium-ion battery (LIB) leachate was successfully demonstrated. The LNMO electrode exhibited selective recovery of lithium from a solution containing various LIB materials, such as Mn, Co, Ni, Cu, Al, Mg, and Fe, as confirmed through tests involving different operating currents and times. The results indicated that electrochemical lithium recovery was achievable at a current density of 0.125 A/g and an operating time of 20 min/step. Furthermore, over 20 cycles, the LNMO electrode showed more stable performance compared to the pristine LMO electrode. The stability of the LNMO electrode further improved with increasing nickel doping. Because of its superior performance, LNMO has the potential to be utilized as a material for long-term selective lithium recovery from actual LIB leachate. In addition, this electrochemical method appears promising for future lithium recovery from end-of-life LIB leachate.

# References


1 Battistel, A., Palagonia, M. S., Brogioli, D., La Mantia, F., & Trócoli, R. (2020). Electrochemical Methods for Lithium Recovery: A Comprehensive and Critical Review . *Advanced Materials*, *32*(23), 1905440.

2 Capsoni, D., Bini, M., Chiodelli, G., Massarotti, V., Azzoni, C. B., Mozzati, M. C., & Comin, A. (2001). Inhibition of Jahn–Teller cooperative distortion in LiMn2O4 spinel by transition metal ion doping [10.1039/B100080M]. *Physical Chemistry Chemical Physics*, *3*(11), 2162-2166.

3 Chemelewski, K. R., Lee, E.-S., Li, W., & Manthiram, A. (2013). Factors Influencing the Electrochemical Properties of High-Voltage Spinel Cathodes: Relative Impact of Morphology and Cation Ordering. *Chemistry of Materials*, *25*(14), 2890-2897.

4 Chen, M., Wu, R., Ju, S., Zhang, X., Xue, F., & Xing, W. (2018). Improved performance of Al-doped LiMn2O4 ion-sieves for Li+ adsorption. *Microporous and Mesoporous Materials*, *261*, 29-34.

5 dos Santos Junior, G. A., Fortunato, V. D. S., Bastos, G. A. A., Silva, G. G., Ortega, P. F. R., & Lavall, R. L. (2020). High-Performance Lithium-Ion Hybrid Supercapacitors Based on Lithium Salt/Imidazolium Ionic Liquid Electrolytes and Ni-Doped LiMn2O4 Cathode Materials. *ACS Applied Energy Materials*, *3*(9), 9028-9039.

6 Guan, D., Jeevarajan, J. A., & Wang, Y. (2011). Enhanced cycleability of LiMn2O4 cathodes by atomic layer deposition of nanosized-thin Al2O3 coatings [10.1039/C0NR00939C]. *Nanoscale*, *3*(4), 1465-1469.

7 Haruna, A. B., Barrett, D. H., Rodella, C. B., Erasmus, R. M., Venter, A. M., Sentsho, Z. N., & Ozoemena, K. I. (2022). Microwave irradiation suppresses the Jahn-Teller distortion in Spinel LiMn2O4 cathode material for lithium-ion batteries. *Electrochimica Acta*, *426*, 140786.

8 Jang, Y., Hou, C.-H., Park, S., Kwon, K., & Chung, E. (2021). Direct electrochemical lithium recovery from acidic lithium-ion battery leachate using intercalation electrodes. *Resources, Conservation and Recycling*, *175*, 105837.

9 Kanoh, H., Ooi, K., Miyai, Y., & Katoh, S. (1993). Electrochemical Recovery of Lithium Ions in the Aqueous Phase. *Separation Science and Technology*, *28*(1-3), 643-651.

10 Kim, S., Lee, J., Kang, J. S., Jo, K., Kim, S., Sung, Y.-E., & Yoon, J. (2015). Lithium recovery from brine using a λ-MnO2/activated carbon hybrid supercapacitor system. *Chemosphere*, *125*, 50-56.

11 Lawagon, C. P., Nisola, G. M., Cuevas, R. A. I., Torrejos, R. E. C., Kim, H., Lee, S.-P., & Chung, W.-J. (2019). Li1−xNi0.5Mn1.5O4/Ag for electrochemical lithium recovery from brine and its optimized performance via response surface methodology. *Separation and Purification Technology*, *212*, 416-426.

12 Lee, J., & Chung, E. (2020). Lithium recovery by solvent extraction from simulated shale gas produced water – Impact of organic compounds. *Applied Geochemistry*, *116*, 104571.

13 Lee, J., Yu, S.-H., Kim, C., Sung, Y.-E., & Yoon, J. (2013). Highly selective lithium recovery from brine using a λ-MnO2–Ag battery [10.1039/C3CP50919B]. *Physical Chemistry Chemical Physics*, *15*(20), 7690-7695.

14 Lee, K., Yang, G. J., & Kim, Y. (2017). Improvement of the electrochemical properties of LiNi0.5Mn1.5O4 by controlling the heating atmosphere during synthesis. *Ceramics International*, *43*(17), 15510-15518.

15 Liu, D.-F., Sun, S.-Y., & Yu, J.-G. (2019). A new high-efficiency process for Li+ recovery from solutions based on LiMn2O4/λ-MnO2 materials. *Chemical Engineering Journal*, *377*, 119825.

16 Ouyang, C. Y., Shi, S. Q., & Lei, M. S. (2009). Jahn–Teller distortion and electronic structure of LiMn2O4. *Journal of Alloys and Compounds*, *474*(1), 370-374.

17 Pasta, M., Battistel, A., & La Mantia, F. (2012). Batteries for lithium recovery from brines [10.1039/C2EE22977C]. *Energy & Environmental Science*, *5*(11), 9487-9491.

18 Porada, S., Zhao, R., van der Wal, A., Presser, V., & Biesheuvel, P. M. (2013). Review on the science and technology of water desalination by capacitive deionization. *Progress in Materials Science*, *58*(8), 1388-1442.

19 Rodríguez, R. A., Pérez-Cappe, E. L., Laffita, Y. M., Ardanza, A. C., Salazar, J. S., Santos, M. Á., Aguilar Frutis, M. A., Mohalem, N. D. S., & Alves, O. L. (2018). Structural defects in LiMn2O4 induced by gamma radiation and its influence on the Jahn-Teller effect. *Solid State Ionics*, *324*, 77-86.

20 Santhanam, R., & Rambabu, B. (2010). Research progress in high voltage spinel LiNi0.5Mn1.5O4 material. *Journal of Power Sources*, *195*(17), 5442-5451.

21 Shang, X., Hu, B., Nie, P., Shi, W., Hussain, T., & Liu, J. (2021). LiNi0.5Mn1.5O4-based hybrid capacitive deionization for highly selective adsorption of lithium from brine. *Separation and Purification Technology*, *258*, 118009.

22 Tabelin, C. B., Dallas, J., Casanova, S., Pelech, T., Bournival, G., Saydam, S., & Canbulat, I. (2021). Towards a low-carbon society: A review of lithium resource availability, challenges and innovations in mining, extraction and recycling, and future perspectives. *Minerals Engineering*, *163*, 106743.

23 Talens Peiró, L., Villalba Méndez, G., & Ayres, R. U. (2013). Lithium: Sources, Production, Uses, and Recovery Outlook. *JOM*, *65*(8), 986-996.

24 Tang, D., Sun, Y., Yang, Z., Ben, L., Gu, L., & Huang, X. (2014). Surface Structure Evolution of LiMn2O4 Cathode Material upon Charge/Discharge. *Chemistry of Materials*, *26*(11), 3535-3543.

25 Thackeray, M. M. (1999). Structural Fatigue in Spinel Electrodes in High Voltage (4 V) Li/Li[sub x]Mn[sub 2]O[sub 4] Cells. *Electrochemical and Solid-State Letters*, *1*(1), 7.

26 Tian, L., & Yuan, A. (2009). Electrochemical performance of nanostructured spinel LiMn2O4 in different aqueous electrolytes. *Journal of Power Sources*, *192*(2), 693-697.

27 Xu, M., Kang, S., Jiang, F., Yan, X., Zhu, Z., Zhao, Q., Teng, Y., & Wang, Y. (2021). A process of leaching recovery for cobalt and lithium from spent lithium-ion batteries by citric acid and salicylic acid [10.1039/D1RA04979H]. *RSC Advances*, *11*(44), 27689-27700.

28 Yu, Y., Guo, J., Xiang, M., Su, C., Liu, X., Bai, H., Bai, W., & Duan, K. (2019). Enhancing the durable performance of LiMn2O4 at high-rate and elevated temperature by nickel-magnesium dual doping. *Scientific Reports*, *9*(1), 16864.

29 Yu, Y. W., Yue; Guo, Junming; Su, Changwei; Liu, Xiaofang; Bai, Xiaofang; Bai, Hongli; Wang. Rui. (2018). Facile Synthesis of Ni-doped Nano-LiMn2O4 ($0 \leq x \leq 0.10$) Cathode

Materials and Their Electrochemical Performances. *International Journal of Electrochemical Science*, *13*.

30 Yuan, A., Tian, L., Xu, W., & Wang, Y. (2010). Al-doped spinel LiAl0.1Mn1.9O4 with improved high-rate cyclability in aqueous electrolyte. *Journal of Power Sources*, *195*(15), 5032-5038.

# 논문초록

리튬(Li)은 리튬이온전지(LIB)와 같은 에너지 관련 응용 분야에서 활용도가 높아 전기화학적 성능이 우수한 것으로 알려져 왔습니다. 일반적으로 수명이 다한 LIB는 리튬 및 기타 LIB 물질을 포함하는 LIB 침출액으로 알려진 용액을 생성하는 침출 공정을 통해 재활용을 수행합니다. LIB 침출액으로부터 리튬을 선택적으로 회수하는 다양한 기술 중에서 일반적으로 LMO 전극을 사용하는 전기화학적 기술은 유망한 기술 중 하나입니다. 그러나 LMO의 안정성 성능은 주로 LMO에서 $Mn^{3+}$의 Jahn-Teller 효과 때문에 좋지 않습니다. 본 연구에서는 LMO의 망간함량을 감소시키기 위하여 니켈도판트로 치환하는 것에 중점을 두었으며, LNMO과 활성탄(AC) 전극을 사용하여 실제 LIB 침출수에서 리튬을 선택적으로 회수하였습니다. LIB 침출수로부터 리튬 회수에 대한 운전시간과 전류의 영향을 연구하여 최적 운전조건을 결정하였습니다. 결과는 긴 작동 시간과 높은 전류가 리튬 포획 용량을 증가시키고 에너지 소비를 증가시킨다는 것을 보여줍니다. 얻어진 최적의 운전조건을 이용한 리튬 회수 시험 결과, 리튬 포획 용량은 1.58 mmol/g, 리튬 순도는 95.22%, 에너지 소비량은 2.79 Wh/mol로 나타났다. 또한, LMO에 니켈 도핑이 성능에 미치는 영향도 20 사이클에 걸쳐 조사되었습니다. 20사이클 리튬 회수 시험에서, LiNi0.5Mn1.5O4(LNMO-0.5) 전극은 안정적인 리튬 회수 성능을 보여 초기 리튬 포획 용량의 약 97%를 유지하고 20사이클 후에는 에너지 소비량을 약 7%

증가시켰습니다. 반면, LMO의 경우 20사이클 후 초기 리튬 포획 용량의 약 47%만이 유지되었으며, 에너지 소비량은 초기 사이클보다 약 65% 더 높았습니다. LNMO의 우수한 성능으로 인해 실제 리튬 이온 배터리 응용 분야에서 침출수로부터 장기 선택적 리튬 회수를 위한 잠재적 재료로 기대됩니다

**Keyword :** 리튬 회수, 전기화학, LIB 침출액, LNMO, 리튬 배터리

**학번 :** 2021-27252